International Journal of Bifurcation and Chaos, Vol. 10, No. 7 (2000) 1759–1772

ANALYSIS OF A NONSYNCHRONIZED SINUSOIDALLY DRIVEN DYNAMICAL SYSTEM

O. MÉNARD, C. LETELLIER, J. MAQUET, L. LE SCELLER and G. GOUESBET
CORIA UMR 6614, Université et INSA de Rouen,
Place Emile Blondel, 76821 Mont Saint-Aignan cedex, France

Received June 30, 1999; Revised December 7, 1999

A nonautonomous system, i.e. a system driven by an external force, is usually considered as being phase synchronized with this force. In such a case, the dynamical behavior is conveniently studied in an extended phase space which is the product of the phase space $\mathbb{R}^m$ of the undriven system by an extra dimension associated with the external force. The analysis is then performed by taking advantage of the known period of the external force to define a Poincaré section relying on a stroboscopic sampling. Nevertheless, it may so happen that the phase synchronization does not occur. It is then more convenient to consider the nonautonomous system as an autonomous system incorporating the subsystem generating the driving force. In the case of a sinusoidal driving force, the phase space is $\mathbb{R}^{m+2}$ instead of the usual extended phase space $\mathbb{R}^m \times S^1$. It is also demonstrated that a global model may then be obtained by using $m+2$ dynamical variables with two variables associated with the driving force. The obtained model characterizes an autonomous system in contrast with a classical input/output model obtained when the driving force is considered as an input.

1. Introduction

When one is facing a dynamical system, it is of interest to know whether the system is driven or not by an external force because, if a driving force is identified, the analysis may take advantage of a possible phase synchronization between the driven system and the external force. Examples are provided by the Duffing equations [Gilmore & McCallum, 1995] or by experimental driven systems such as a driven laser [Boulant *et al.*, 1997] or a driven thermoionic plasma diode [Mansbach *et al.*, 1999]. When the driving force is identified, the phase space $\mathbb{R}^m$ of the undriven system is usually extended to $\mathbb{R}^{m+1}$ to describe the driven system. In such a case, the analysis relies on the use of stroboscopic sections to compute Poincaré sections and to extract periodic orbits [Gilmore & McCallum, 1995; Boulant *et al.*, 1997]. The system is therefore implicitly considered as being phase synchronized with the driving force. Moreover, when the driving force may be recorded simultaneously with a dynamical variable of the system, an input/output model can be obtained [Aguirre & Billings, 1994]. A set of equations is then built to describe the response of the system under the action of the driving force.

Nevertheless, it may occur that the system is not well phase synchronized with the driving force. In other cases, the driving force cannot be identified or cannot be measured. Under such circumstances, a dynamical analysis cannot be safely performed in the extended phase space $\mathbb{R}^{m+1}$ and the use of a higher-dimensional phase space becomes more convenient. Such a phase space is spanned by the dynamical variables required for a complete description of the process governing both the driven system and the driving force. A driven Rössler system, with a driving force applied to the third equation, is used in this paper to illustrate a situation where a system is not well phase synchronized with the driving force and, a single variable being recorded, where the driving force cannot be measured.

The paper is organized as follows. Section 2 provides a brief review on global modeling and topological characterization. Section 3 describes the case of a Duffing oscillator which is phase synchronized with the external force. Section 4 is devoted to a driven Rössler system whose synchronization with the driving force depends on its amplitude. Section 5 is the conclusion.

2. Mathematical Background

2.1. *Dynamical systems*

We consider a dynamical system defined by a set of ordinary differential equations reading as:

$$\dot{\mathbf{x}} = \mathbf{G}(\boldsymbol{\mu}, \mathbf{x}, t) \tag{1}$$

in which $\mathbf{x} \in \mathbb{R}^m$ is the state vector, $\mathbf{G}$ is a vector valued function, $\boldsymbol{\mu} \in \mathbb{R}^p$ is the control parameter vector and $\mathbf{G}$ is the vector field. When the vector field explicitly depends on time t, the system is *nonautonomous*. In the converse case, it is *autonomous*. In any case, $\mathbf{G}$ is a m-component smooth function generating a flow ϕ_t defined as:

$$\begin{cases} \phi_t : \ \mathbb{R}^m \times \mathbb{R} \to \mathbb{R}^m \\ \phi_t(\mathbf{x}_0, t) = \mathbf{x}_t \quad \text{for every } \mathbf{x}_0 \in \mathbb{R}^m \text{ and } t \in \mathbb{R} \end{cases} \tag{2}$$

where $\mathbf{x}_0$ is the initial condition at $t_0 = 0$ and $\mathbf{x}_t$ represents the trajectory in the phase space.

A volume V of initial conditions is generally not invariant along flows. The rate of change of V may be quantified by using the Lie derivative [Bergé *et al.*, 1984]. When it is negative, the flow is *dissipative* and the asymptotic motion settles down onto an attractor $\mathcal{A}$ defined as follows.

Definition 1. A closed and bounded invariant set $\mathcal{A}$ is said to be an attractor if there is a neighborhood $\mathcal{U}(\mathcal{A})$ such that for every $\mathbf{x} \in \mathcal{U}(\mathcal{A})$, $\phi_t(\mathbf{x}, t) \in \mathcal{U}(\mathcal{A})$ for positive times and $\lim_{t\to\infty} \phi_t(\mathbf{x}, t) = \mathcal{A}$.

When a dynamical system is driven by an external force, it may be viewed as constituted by a dissipative subsystem interacting with a Hamiltonian process. There is then a continuum of attractors since, to each set of initial conditions for the Hamiltonian process, i.e. the driving force, corresponds a different attractor for the dissipative subsystem. We say that such a system is *mixed*. Examples and justifications for these definitions will appear in the sequel.

2.2. *Global modeling*

Given a scalar time series $\{x_i\}_{i=1}^N$, it has been shown that a set of equations may be built starting from the series [Crutchfield & McNamara, 1987; Farmer & Sidorowitch, 1987]. The variables involved in the model may equivalently rely on time-delay coordinates or derivatives. Here, the derivative coordinates are used as in [Gouesbet & Letellier, 1994]. The successive derivatives $\dot{x}(t)$, $\ddot{x}(t), \ldots$ of the time series are evaluated to form vectors ($X_1 = x$, $X_2 = \dot{x}, \ldots, X_{d_E} = d^{d_E-1}x/dt^{d_E-1}$) defining the state of the system in a d_E-dimensional space. We then model the dynamics by using a vector field reading as [Gouesbet & Maquet, 1992]:

$$\begin{cases} \dot{X}_1 = X_2 \\ \dot{X}_2 = X_3 \\ \vdots \\ \dot{X}_{d_E} = F(X_1, X_2, \ldots, X_{d_E}) \end{cases} \tag{3}$$

where F is a function to estimate.

The function F is approximated by using a mutivariate polynomial basis on nets [Gouesbet & Letellier, 1994] which may be built by means of a Gram–Schmidt orthogonalization procedure [Letellier *et al.*, 1997]. It is important here to stress that the use of a polynomial basis is not an essential ingredient for estimating the function F. Rational functions, or other models, may work too ([Gouesbet & Maquet, 1992] and references therein). However, even if the function F is not exactly a polynomial, the Weierstrass convergence theorem [Rice, 1964, 1969] tells us that the function F may, in principle, be arbitrary closely approximated by polynomial forms, explaining why global vector field modeling have been successfully applied to many experimental, even noisy, systems [Crutchfield & McNamara, 1987; Brown *et al.*, 1994; Letellier *et al.*, 1995]. The use of polynomials in this paper therefore does not constitute a noticeable limitation of its contents. Let us however remark that exact functions used in this paper will be polynomials, allowing one to stress on physics without being possibly disturbed by numerical incidental difficulties.

The polynomial algorithm uses modeling parameters which are (i) d_E, the embedding dimension, (ii) N_v, the number of vectors

$(X_{1,i}, X_{2,i}, \ldots, X_{d_E,i})$, $(i \in [1, N_v])$ on the net, with i a time index, (iii) Δt, the time step between two successive vectors which may be expressed as the number of vectors, N_p, sampled per pseudo-period, (iv) N_K, the number of retained multivariate polynomials and (v) τ_w, the window size on which the derivatives are estimated (by using a sixth degree interpolation polynomial). Here, $\tau_w = 7\delta t$ where δt is the time step used in the discretization of the time series. The interpolation polynomials are built by using six nearest neighbors. Derivatives are obtained by analytically deriving these polynomials. Of course, it is well known that using higher derivatives amplifies numerical errors. The present method to evaluate derivatives is however very efficient. In particular, as a consequence, the present global modeling technique with derivatives has been successfully applied to many experimental systems [Crutchfield & McNamara, 1987; Letellier *et al.*, 1995]. The estimated function, denoted $\tilde{F}$, finally reads as:

$$\tilde{F}(X_1, X_2, \ldots, X_{d_E}) = \sum_{p=1}^{N_K} K_p \Xi^p \qquad (4)$$

where $\Xi^p = X_1^{n_1} X_2^{n_2} \cdots X_{d_E}^{n_{d_E}}$ is a monomial in which the integers p are related to n_{d_E}-uplets $(n_1, n_2, \ldots, n_{d_E})$ by a bijective relationship [Gouesbet & Letellier, 1994].

It is not always ensured that we can obtain a sufficiently good approximation to the function F, due, for instance, to numerical uncertainties. Such a difficulty is enhanced for nonautonomous systems because the time t may be involved in the function F. Since it does not vary on a bounded range, there is no recurrence property in the extended phase space and therefore it is very difficult, or even impossible, to obtain a sufficiently good approximation $\tilde{F}$. Global modeling then leads to systems which eventually diverge. An alternative approach will be later presented. The faithfulness of a model may be checked by using symbolic dynamics and linking numbers as described in the next section.

As a last remark in this subsection, let us mention that the number of vectors N_v, used for the modeling process, may be in some cases, only slightly larger than the number of parameters, N_K, to be estimated. Such a feature is observed for very favorable cases when, for instance, there is no noise in the simulated data. When the data are noise corrupted, the number of vectors N_v may be increased as well as the number of coefficients retained in the estimated function $\tilde{F}$. Nevertheless, it is often observed that, when the number of vectors N_v is increased too much, the quality of the model may decrease as the result of enhanced numerical uncertainties which degrade the quality of the estimated function $\tilde{F}$, i.e. there may be some optimal values of N_v.

2.3. *Symbolic dynamics and topological characterization*

It is useful to transform continuous flows into discrete-time maps by introducing a Poincaré section allowing one to compute a first-return map [Wiggins, 1980]. The Poincaré section is the set of intersections between the trajectory generated by the m-dimensional system under study with an $(m-1)$-dimensional surface Σ transverse to the vector field $\mathbf{G}$. The first-return map is split into N elements, labeled by symbols $\sigma \in \Sigma_N = \{0, \ldots, N-1\}$, and each orbit $x_1, \ldots, x_n$ is associated with a symbol sequence $\sigma_1, \ldots, \sigma_n$ by using a generating partition. If the flow lies in $\mathbb{R}^3$ and is strongly dissipative, the first-return map is nearly one-dimensional. An approximate generating partition is then defined by critical points associated with local extrema separating monotonic branches. Each branch is associated with a symbol. The case of weakly dissipative systems is more complicated [Flepp *et al.*, 1991; Fang, 1995; Grassberger *et al.*, 1989].

In the case of a strongly dissipative 3D system whose first-return map is unimodal with a differentiable maximum, all trajectories are encoded on the set $\Sigma_2 = \{0, 1\}$ where 0 is associated with the increasing branch and 1 with the decreasing branch. A period-q orbit has q periodic points in a Poincaré section and is represented by a string $S = \sigma_1\sigma_2\cdots\sigma_q$ of q symbols. Each periodic point is represented by a symbolic sequence of q symbols too. The ith point of a period-q orbit is labeled by the string $S_i = \sigma_i\sigma_{i+1}\cdots\sigma_q\sigma_1\cdots\sigma_{i-1}$. All symbolic sequences are ordered by the unimodal order [Collet & Eckmann, 1980; Hall, 1994].

Definition 2. To define the unimodal order $\prec_1$ on the symbol set $\Sigma_2 = \{0, 1\}$, we consider two symbolic sequences $S_1 = \sigma_1\sigma_2\cdots\sigma_k\sigma_{k+1}\cdots$ and $S_2 = \rho_1\rho_2\cdots\rho_k\rho_{k+1}\cdots$ where σ_i's and ρ_j's designate the symbols of Σ_2. Assume $\sigma_i = \rho_i$ for all $i < k$ and $\sigma_k \neq \rho_k$. Let $S^* = \sigma_1\sigma_2\cdots\sigma_{k-1} = \rho_1\rho_2\cdots\rho_{k-1}$ be the common part of S_1 and S_2. A

string $\sigma_1\sigma_2\cdots\sigma_{k-1}$ is even (odd) if the sum $\sum_{i=1}^{k-1}\sigma_i$ is even (odd). Then, we have:

$$\begin{cases} S_1 \prec_1 S_2 & \text{if } S^* \text{ is even and } \sigma_k < \rho_k \\ S_1 \prec_1 S_2 & \text{if } S^* \text{ is odd and } \rho_k < \sigma_k \\ S_2 \prec_1 S_1 & \text{if } S^* \text{ is odd and } \sigma_k < \rho_k \\ S_2 \prec_1 S_1 & \text{if } S^* \text{ is even and } \rho_k < \sigma_k \end{cases}$$

where $<$ is the natural order on the integers. When $S_2 \prec_1 S_1$, we say that S_1 implies S_2.

A period-q orbit is denoted by the symbolic sequence S_i (without any parentheses) which implies $q-1$ others. This sequence is designated by (S_i), included between parentheses, and called the *orbital sequence*. Two orbital sequences may be ordered following the unimodal order too. When an orbital sequence (S_1) implies the orbital sequence (S_2), we say that (S_1) *forces* (S_2) and we note $(S_2) \prec_2 (S_1)$ where $\prec_2$ is the forcing order. The orbital sequence which forces all orbital sequences of an attractor is called the *kneading sequence*. The unimodal order may be generalized to the case $N > 2$ [Dutertre, 1995].

When dealing with experimental data, the periodic orbits are extracted from a time series by using a close return method in a reconstructed phase space. Due to the limited amount of data and the influence of external noise, the determination of the kneading sequence is rather inaccurate for short time series [Tufillaro *et al.*, 1995]. An empirical procedure may however allow one to determine the kneading sequence [Tufillaro *et al.*, 1995; Fang, 1994] as described below.

A chaotic trajectory forms a string $S = \cdots\sigma_{-3}\sigma_{-2}\sigma_{-1}\sigma_0\sigma_1\sigma_2\sigma_3\cdots$ where σ_0 is the present, σ_{-i} the past and σ_i the future $(i > 0)$. Symbolic coordinates spanning a symbolic plane are then defined on the future and on the past by:

$$\begin{cases} x_\sigma(\mathbf{s}) = \displaystyle\sum_{i=1}^{D} \frac{b_i}{N^i} & \text{where } b_i = \displaystyle\sum_{j=1}^{i} \sigma_j \pmod 2 \\ y_\sigma(\mathbf{s}) = \displaystyle\sum_{i=1}^{D} \frac{c_i}{N^i} & \text{where } c_i = \displaystyle\sum_{j=0}^{i-1} \sigma_{-j} \pmod 2 \end{cases} \tag{5}$$

where

$$\mathbf{s} = \sigma_{-D}\cdots\sigma_{-3}\sigma_{-2}\sigma_{-1}\sigma_0\sigma_1\sigma_2\sigma_3\cdots\sigma_D \tag{6}$$

If $\mathbf{s}$ is an infinite string generated by a chaotic orbit, then D is infinity. For finite data sets, the symbolic plane coordinates are approximated by taking $D = 16$ [Tufillaro *et al.*, 1995]. We can then use a finite symbol string from a chaotic trajectory to generate a sequence of points in the symbolic plane. This symbolic plane exhibits a maximum symbolic coordinate X_σ which is associated with the kneading sequence.

In the case of a unimodal map, the chaotic attractor may be divided into two strips, one with an even number of half-twists (rotations by π) associated with the increasing branch of the first-return map and the other with an odd number of half-twists corresponding to the decreasing branch. The topological organization of strips may be synthetized by a template defined in [Mindlin *et al.*, 1991; Mindlin & Gilmore, 1992].

The template may be algebraically described by using a linking matrix [Tufillaro *et al.*, 1992]. Diagonal elements M_{ii} are equal to the number of half-twists of the ith strip and off-diagonal elements M_{ij} $(i \neq j)$ are given by the algebraic number of intersections between the ith and the jth strips. One example is the horseshoe template defined by the linking matrix:

$$M \equiv \begin{bmatrix} 0 & 0 \\ 0 & +1 \end{bmatrix} \tag{7}$$

Next, linking numbers are defined as follows:

Definition 3. Let α and β be two knot diagrams. Let $\alpha \sqcap \beta$ denote the set of crossings of α with β. The linking number reads as:

$$lk(\alpha, \beta) = \frac{1}{2} \sum_{p \in \alpha \sqcap \beta} \varepsilon(p) \tag{8}$$

where $\varepsilon(p)$ is the sign of the crossing p.

The linking numbers may be predicted by constructions on the template or by an algebra based on the linking matrix [Le Sceller *et al.*, 1994]. The compatibiliy of a template with an attractor may be checked by comparing linking numbers predicted by the template and the ones counted on plane projections of couples of periodic orbits extracted from the attractor.

3. Global Phase Space for the Duffing Equation

The Duffing equations are usually investigated in a 3D phase space, i.e. in an extended phase space

$\mathbb{R}^2 \times S^1$ accounting for the existence of the driving force. We will show that, when the driving force is not recorded, a 4D phase space may conveniently be used.

3.1. *Extended phase space*

The Duffing equation reads as:

$$\ddot{x} + a\dot{x} + x^3 = A\,\cos(\omega t + \varphi) \tag{9}$$

where a is the dissipative rate of energy, A the amplitude of the driving force $F(t) = A\,\cos(\omega t + \varphi)$, ω its frequency and φ its phase. This equation may be rewritten as a set of first-order ordinary differential equations as follows:

$$\begin{cases} \dot{x} = y \\ \dot{y} = -ay - x^3 + A\,\cos(\omega t + \varphi) \end{cases} \tag{10}$$

This nonautonomous system is usually converted to an autonomous system reading as:

$$\begin{cases} \dot{x} = y \\ \dot{y} = -ay - x^3 + A\,\cos(\nu) \\ \dot{\nu} = \omega \end{cases} \tag{11}$$

However, let us assume that we only know a single scalar time series $x(t)$ and that the existence of a driving force is not identified. The embedding dimension may then be estimated by using a false nearest neighbor method. This method has been introduced in [Abarbanel & Kennel, 1993] but a recent algorithm [Cao, 1997] is here preferred. The embedding dimension is thus found to be equal to 4 rather than 3 (Fig. 1), as would be expected from Eqs. (11). Such a result may be understood as follows. A representation on a space $\mathbb{R}^2 \times (\mathbb{R} \bmod (2\pi/\omega))$ provides a compact attractor but such a representation requires a prior knowledge of ω which is here assumed to be unknown. This is also in agreement with the fact that, if a model is searched by using the global modeling technique described in the previous section, no model is obtained by using a 3D reconstructed state space spanned by derivative coordinates $(X, Y, Z) = (x, \dot{x}, \ddot{x})$.

When a global system involving the driving force is to be modelized in $\mathbb{R}^3$, the $\cos(\nu)$ term of Eq. (11) must be approximated directly on the chosen basis. This leads to a slow convergence and to a rather poor approximation [Crutchfield & McNamara, 1987]. The existence of terms explicitly involving the time t is a signature of the fact that

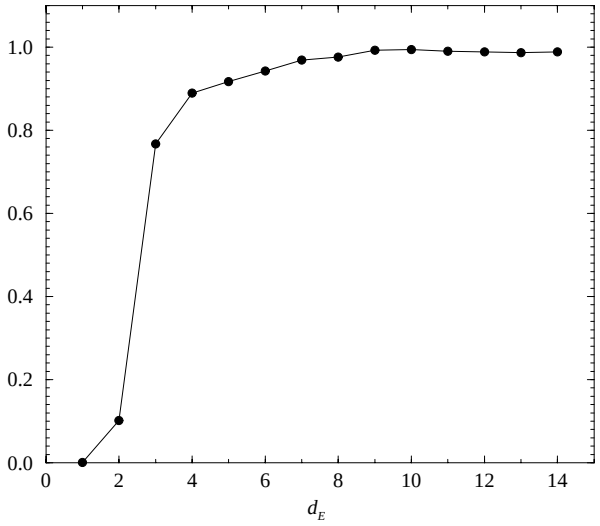

Fig. 1. Embedding dimension computed from the x-variable of the Duffing equations. In the method proposed by Cao, the ordinates saturate when the embedding dimension is sufficiently large. The embedding dimension is greater than 3 and may be well estimated to be equal to 4. The control parameters $(a, b) = (0.05, 7.5)$. The time step δt is equal to 0.02 s and the time delay is equal to 18 δt.

there are some dynamical processes generating the driving force which are not explicitly described by the vector field (11). In other words, the driving force is described by kinetic terms rather than by a dynamical model. Other dynamical variables must be added as indicated by the embedding dimension being equal to 4. Indeed, the driven system may be extended to a larger autonomous system by including additional equations describing the driving force. The extended phase space is then replaced by a global phase space.

3.2. *Global phase space*

The external sinusoidal driving force $A\,\cos(\omega t - \varphi)$ is generated by a second-order differential equation. The nonautonomous Duffing system may then be rewritten as an autonomous four-variable system reading as:

$$\begin{cases} \dot{x} = y \\ \dot{y} = -ay - x^3 + u \\ \dot{u} = v \\ \dot{v} = -\omega^2 u \end{cases} \tag{12}$$

which is in agreement with the value of the embedding dimension obtained from false nearest neighbors. An important difference with respect to

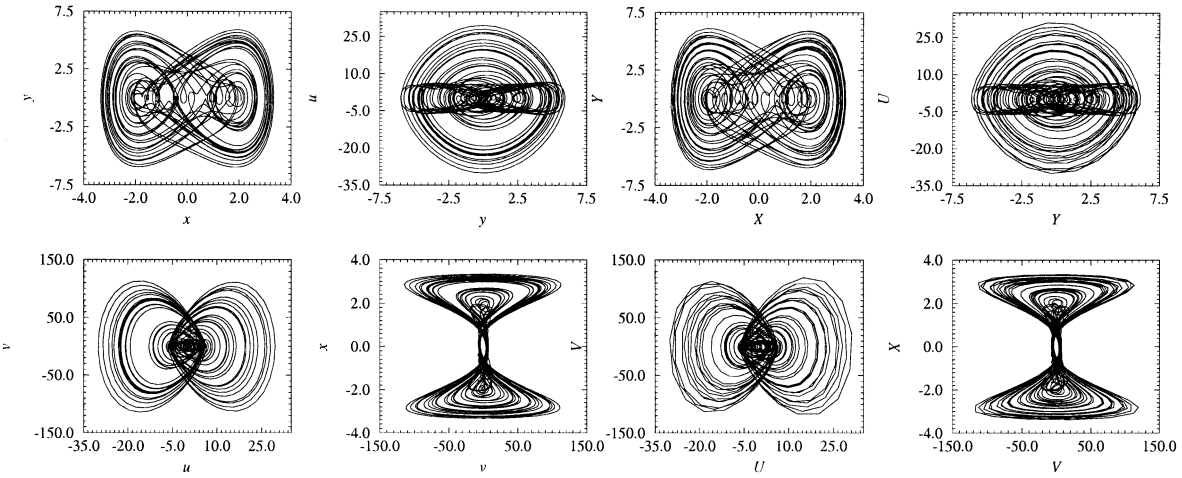

(a) Duffing system. (b) 4D model.

Fig. 2. Four of the six plane projections of the phase portrait generated by the four-variable Duffing system.

usual autonomous systems is that the two dynamical variables (u, v) are associated with a conservative dynamical process having a Hamiltonian function $H(u, v) = (1/2)[\omega^2 u^2 + v^2]$. Therefore, strictly speaking, there is no attractor in the global phase space because, if we change (u_0, v_0), the asymptotic motion changes too. Since the two other dynamical variables (x, y) remain associated with dissipative processes, we are facing a continuum of attractors. The global system is a mixed one.

Relying on the embedding dimension d_E being equal to 4, a model is attempted by using a 4D reconstructed space spanned by $(X, Y, U, V) = (x, \dot{x}, \ddot{x}, \dddot{x})$. The model takes the form given by Eq. (3). A successful model is obtained with modeling parameters $(N_v, N_p, N_K) = (30, 20, 20)$. The model portrait is obtained by integrating the model and is displayed in Fig. 2(b), to be compared with the original phase portrait displayed in Fig. 2(a). In such a case, the exact function $F(X, Y, U, V)$ may be analytically derived to check the model and reads as:

$$\begin{cases} \dot{X} = Y \\ \dot{Y} = U \\ \dot{U} = V \\ \dot{V} = -aV - 6XY^2 - \omega^2 U - a\omega^2 Y - \omega^2 X^3 - 3X^2 U \\ \quad = F(X, Y, U, V) \end{cases} \tag{13}$$

The estimated function $\tilde{F}(X, Y, U, V)$ obtained by the global modeling technique has coefficients which differ from the exact coefficients involved in system (13) with a relative error less than 0.004%. No other validation is therefore required. Nevertheless, a validation without any knowledge about the original set of equations could be given as described in [Gilmore & McCallum, 1995]. The global modeling technique has therefore been successfully applied by using an additional variable, i.e. by describing the dynamics in a 4D global phase space rather than in a 3D extended phase space. The use of a global phase space also allows one to get rid of the double status of time exhibited in the extended system (11).

4. Characterization of the Driven Rössler System

The Duffing system is phase synchronized with the driving force and therefore constitutes a very favorable case. Our aim is now to investigate a more complicated case for which the phase synchronization between the system and the driving force is not always guaranteed. A modified Rössler system in which a driving force is applied to the third equation is used. It reads as:

$$\begin{cases} \dot{x} = -y - z \\ \dot{y} = x + ay \\ \dot{z} = b + z(x - c) + A\cos(\omega t + \varphi) \end{cases} \tag{14}$$

where the control parameters (a, b, c) are fixed to $(0.398, 2.0, 4.0)$. The additional control parameter ω is set to $2\pi/T_0$ where $T_0 \approx 6.2$ s is the pseudo-period of the original Rössler system. The amplitude A of the driving force $F(t)$ is in the range

[0.0, 2.0]. Beyond the upper value of the range, the trajectory crosses the plane defined by the stable manifold of the outer fixed point of the Rössler system. Because this plane defines a boundary of the attraction basin, the trajectory is then ejected to infinity being driven along the eigenvector associated with the positive eigenvalue.

4.1. *Embedding dimension*

We assume that only the time evolution of the y-variable is recorded and that no other knowledge from the dynamics is available. We then start with an estimation of the embedding dimension by using a false-neighbor algorithm [Cao, 1997]. Depending on the amplitude A of the driving force (which is not assumed to be known), different values of the embedding dimension are found (Fig. 3). The phase portrait can be embedded in a 3D space for amplitudes up to 0.45. Beyond this value of the amplitude, the embedding dimension is found to be equal at least to 4. For $A = 1.0$ and $A = 1.25$, the embedding dimension is equal to 5 and, for A further increasing, it decreases back to 4. This nonmonotonic evolution of the embedding dimension versus the amplitude may arise from resonances between the driving force and the original Rössler system. We however conclude that the 5D driven Rössler system is close to a 3D system in the low amplitude case, the driving perturbations being efficiently damped by the driven system while a higher-dimensional embedding space must be used for larger amplitude.

One may remark that the dimension 5 is in fact the natural one since, as for the Duffing system, the driven Rössler system may be rewritten as an autonomous system by increasing its dimension by 2:

$$\begin{cases} \dot{x} = -y - z \\ \dot{y} = x + ay \\ \dot{z} = b + z(x - c) + u \\ \dot{u} = v \\ \dot{v} = -\omega^2 u \end{cases} \tag{15}$$

Here, the driving force is a sinusoidal force. Nevertheless, a generalization to any kind of driving force may obviously be provided by using a sufficiently large number of additional dynamical variables to describe the processes generating the driving force. This number may be considered as being estimated with the aid of a false nearest neighbor method, i.e. $d_E = 3 + d_F$ where 3 refers to the dimension of the Rössler system and d_F to the number of variables required to describe the driving force. We chose to apply the driving force to the third equation of the original Rössler system because, in this case, starting from the y-variable which is the best variable of the Rössler sytem [Letellier & Gouesbet, 1996], the function F is a second-order polynomial with 17 monomials. Therefore, F and $\tilde{F}$ have the same form, leading to an easy modeling. This will facilitate the interpretation of our results. In particular, departures between the model and the original systems will only arise from the kind of information contained in the time series, and not from the modeling technique itself. Also, the map $(x, y, z, u, v) \stackrel{\phi}{\to} (X, Y, Z, U, V)$ defines a diffeomorphism, i.e. the best kind of equivalence that we may obtain by a global modeling [Letellier & Gouesbet, 1996]. Moreover, the fact that F and $\tilde{F}$ share the same structure helps to reduce the sensitivity of the analysis to noise contamination which may increase the number of coefficients N_K to be retained in the estimation of the function F [Letellier, 1994]. Nevertheless, when a global model is obtained from a noisy dynamics, the model usually generates a behavior corresponding more or less to a behavior which would be generated by a dynamics with a reduced noise level as discussed in [Letellier *et al.*, 1995], i.e. the modeling process acts as a noise filtering process.

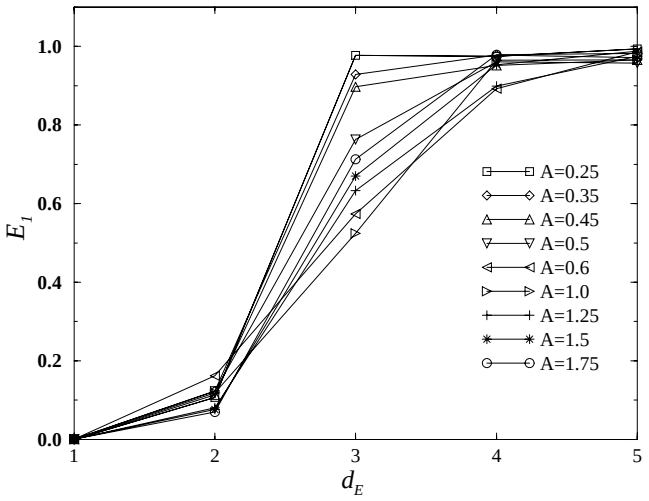

Fig. 3. Evolution of the embedding dimension d_E versus the amplitude A of the driving force applied to the Rössler system. Index $E_1(d)$ measures the relative change in the average distance between two neighbor points in $\mathbb{R}^d$ and their respective images in $\mathbb{R}^{d+1}$ when the embedding dimension is increased from d to $d + 1$. The quantity E_1 stops changing when the embedding dimension is sufficiently large.

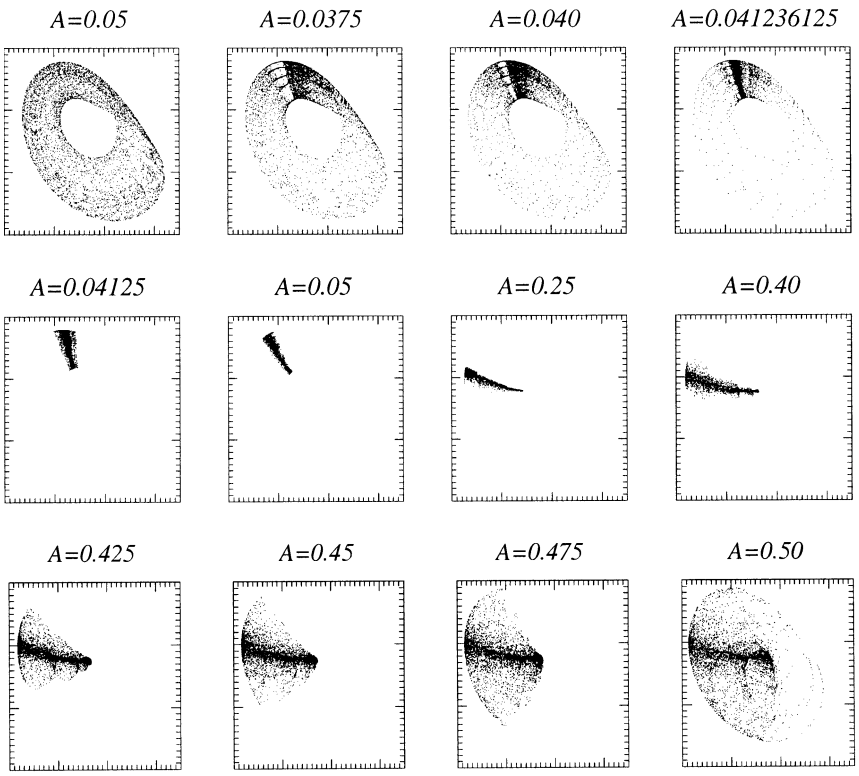

Fig. 4. First-return maps to a delay Poincaré section for different values of the amplitude A. Abscissae are in the range $[-4.5; 6.0]$ and ordinates in the range $[-6.0; 3.0]$.

4.2. *Analysis of the dynamics*

In this subsection, we investigate the dynamics in the original phase space $\mathbb{R}^5$ to later help us to interpret the results obtained with the global modeling technique. All information about the system is assumed to be known in this subsection, i.e. the set of equations is available.

Since a 3D embedding space is sufficient to analyze the Rössler system under the action of a low amplitude driving force ($A = 0.35$), the most natural space is the space spanned by the coordinates (x, y, z) of the original Rössler system since the trajectory in the 2D subspace associated with the Hamiltonian subsystem generating the forcing term corresponds to a periodic orbit, more specifically to a trivial knot which is a very poor object from a topological point of view. We then use a delay Poincaré section in which the behavior depends on the pseudo-period T_0 of the attractor with respect to the period T_F of the driving force. We precisely say that the Rössler and the driving systems are *phase synchronized* when T_0 and T_F are equal. In Fig. 4, top row, the amplitude is small and there is no phase synchronization. The delay Poincaré sections then provide a picture of the whole attractor. For larger amplitudes (middle row), phase synchronization occurs and the pictures approach a single line as it would happen for the unforced Rössler system. This line is however slightly broadened by the effect of the driving force. When the amplitude still increases (bottom row), the dynamics loses its 3D character and is driven to a 5D space. The Poincaré sections then extend again, and present a fuzzy aspect in which some structures may nevertheless be observed. They are however very different from the ones at the top row of Fig. 4.

For $A = 0.35$, the driven Rössler system is characterized by a kneading sequence encoded by (1000) associated with a symbolic coordinate (computed with $N = 3$) equal to 0.6585 to be compared with the kneading sequence (10111101010) and its symbolic coordinate 0.6109 for the undriven system. The population of periodic orbits extracted from the driven Rössler system is reported in Table 1. Many linking numbers have been evaluated on plane projections of pairs of periodic orbits and are well predicted by a linking matrix reading as:

$$M \equiv \begin{bmatrix} 0 & -1 \\ -1 & -1 \end{bmatrix} \tag{16}$$

Table 1. Population of periodic orbits with i period less than 7 for $A = 0.35$. They are identified by their orbital sequence (W). The population for the models are also reported. • indicate that a periodic orbit is embedded within the corresponding attractor.

(W)	Original System	3D Model	5D Model
(1)	•	•	•
(10)	•	•	•
(1011)	•	•	•
(101110)	•	•	•
(101111)	•	•	•
(10111)	•	•	•
(10110)	•	•	•
(101)	•	•	•
(100)	•		•
(100101)	•		•
(10010)	•		•
(10011)	•		•
(100111)	•		•
(100110)	•		•
(1001)	•		•
(1000)	•		•

For a larger amplitude ($A = 0.6$), the dissipation rate of the system is not sufficient any longer to damp the effect of the driving force along the stable manifold during one revolution on the attractor and the embedding dimension is greater than 3. The chaotic trajectory cannot any more be viewed as traveling on a very thin stretched and folded band. A signature of this fact may be perceived in Fig. 5 where one observes that the structure of the folding seems to be diffused. The trajectory actually evolves within a band whose thickness is exhibited by a first-return map to a Poincaré section (Fig. 6).

For such a first-return map, the generating partition is not well defined by a single critical point but rather by a partition line determined from the tangencies of forward and backward foliations [Flepp *et al.*, 1991; Fang, 1995; Grassberger *et al.*, 1989]. Such a determination is not trivial and out of the scope of this paper. We then use partition lines defined by extrema of the first-return map as displayed in Fig. 6.

The first-return map exhibits a third (increasing) monotonic branch inducing a third strip on the

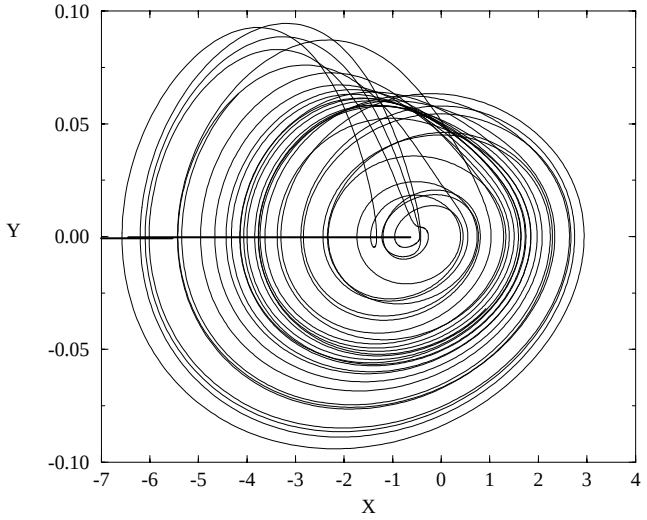

Fig. 5. Plane projection of the driven Rössler system for $A = 0.6$.

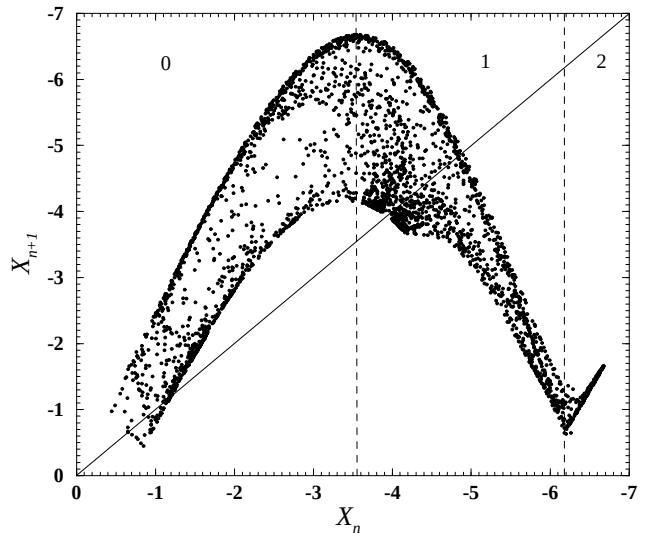

Fig. 6. First-return map to a Poincaré section of the driven Rössler system for $A = 0.6$.

template. Its linking matrix reads as:

$$M_{ij} \equiv \begin{bmatrix} 0 & -1 & -1 \\ -1 & -1 & -2 \\ -1 & -2 & -2 \end{bmatrix} \tag{17}$$

All linking numbers computed in the (x, y, z) space have been found to be in agreement with linking numbers predicted by the three-strip template. Topological properties are therefore not deeply modified by the driving force, at least for low periodic orbits. The population of periodic orbits in the space spanned by (x, y, z) is reported in

Table 2. Population of periodic orbits for the driven Rössler system with $A = 0.6$. They are identified by their orbital sequence (W). Populations of 3D- and 5D-models are also reported.

(W)	Original System	3D Model	5D Model	(W)	Original System	3D Model	5D Model
(0)	•		•	(10001)	•		•
(1)	•	•	•	(10000)	•		•
(10)	•	•	•	(100001)	•		•
(1011)	•	•	•	(200000)	•		•
(101110)	•	•	•	(200001)	•		•
(101111)	•	•	•	(20000)	•		•
(10111)	•	•	•	(20001)	•		•
(10110)	•	•	•	(200011)	•		•
(101)	•	•	•	(2000)	•		•
(100)	•	•	•	(2001)	•		•
(100101)	•	•	•	(200110)	•		•
(10010)	•		•	(200111)	•		•
(10011)	•		•	(20011)	•		•
(100111)	•		•	(20010)	•		•
(100110)	•		•	(200101)	•		
(1001)	•		•	(200100)	•		
(1000)	•		•	(200100)	•		•
(100020)	•		•	(200)	•		•
(100011)	•		•	(201)	•		•

Table 2. The kneading sequence is encoded by (201) associated with a symbolic coordinate $x_\sigma = 0.7142$. Increasing the amplitude of the driving force therefore develops the population of periodic orbits.

In previous cases, periodic orbits are found to be well encoded by a partition estimated by using lines associated with the extrema of the first-return map. Conversely, for very large amplitudes ($A = 1.00$), specific problems are encountered. As an example, for an amplitude $A = 1.00$, a period-2 orbit, encoded (10) with the above generating partition, has been extracted from a 5D model. A simple visual inspection (Fig. 7) however shows that it rather corresponds to a period-1 orbit encoded by 1 (compare it with the period-2 orbit also encoded (10) and extracted from the driven Rössler system displayed in Fig. 8). Another example of problematic features has been observed, namely the case of a periodic orbit which looks very similar to the correct one but whose periodic points are not correctly located in the Poincaré section. This happens for a period-2 orbit encoded (10) which is displayed in Fig. 9, together with a period-4 orbit encoded (1011). According to the unimodal order, we should have:

$$0111 \prec_1 01 \prec_1 1101 \prec_1 1110 \prec_1 10 \prec_1 1011$$

Conversely, we observe

$$\tilde{01} \prec_1 0111 \prec_1 1101 \prec_1 1110 \prec_1 1011 \prec_1 \tilde{10}$$

as displayed in Fig. 9. Indeed, on a Poincaré section (for instance using $Y = 0$ in Fig. 9), the periodic points of the orbit (10) are located outside of the range spanned by the periodic points of the orbit (1011). Here, $\tilde{01}$ and $\tilde{10}$ designate the badly located periodic points. Such discrepancies with respect to the unimodal order have only been observed for very large amplitudes, and actually are a signature of strong structural modifications induced by a sufficiently big forcing.

4.3. *Global modeling*

The increase in dimension observed in Sec. 4.1 implies that we now have to model the input and the

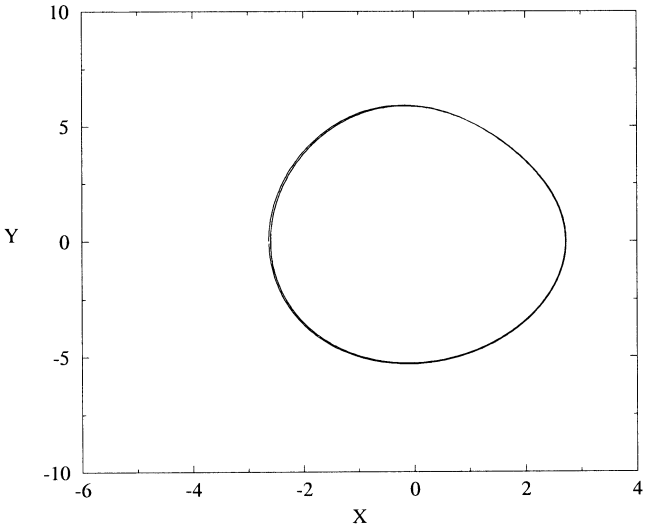

Fig. 7. Period-2 orbit extracted from the 5D model. The two intersections with the Poincaré section are located on each side of and close to the critical point and are therefore encoded 0 and 1, respectively. It however looks like a period-1 orbit. But such an orbit could not be close to the critical point since it is located, for a standard dissipative case, at the intersection between the first-return map and the first bissectrix.

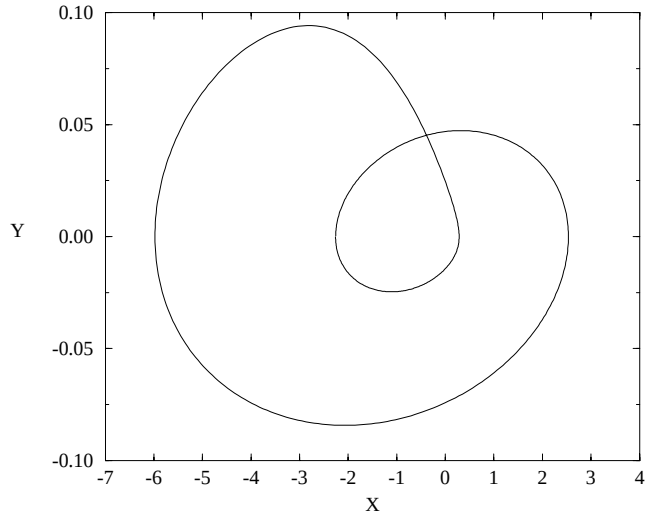

Fig. 8. Period-2 orbit extracted from the driven Rössler system for $A = 1.00$. It is encoded (10).

system as a whole. The model then involves the input. Such an approach is possible when the input is sufficiently simple to be modeled. Of course, when the system is driven by a nonstationary input which cannot be modeled, the analysis discussed here is not practical. In our description, since the input is incorporated in the model, the analysis can only be carried out for attractors of the whole system,

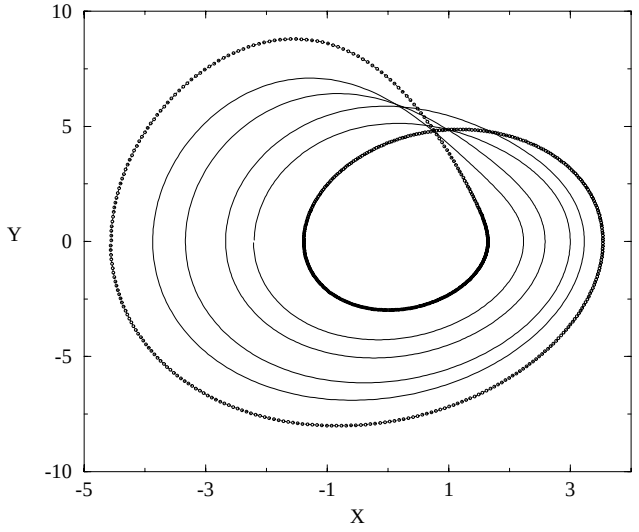

Fig. 9. A period-2 orbit encoded (10) together with a period-4 orbit encoded (1011). The location of periodic points does not satisfy the unimodal order.

i.e. generating the system driven by the input. In particular, an investigation of the change of the output when the input is varied cannot be done with a single model. Indeed, a global model is obtained for a given input and, consequently, generates a single attractor. On the contrary, when an input/output model is estimated, such a model can generate a continuum of attractors by varying the input applied to this model.

We now return to the case when only a single scalar time series is known, i.e. when the input is not measured. Global models in 3D, 4D and in 5D phase spaces are attempted for different amplitude values. In any case, no successful model is obtained by working in a 4D phase space whose dimension is not a natural dimension of the system under study. Indeed, a 3D description corresponds to the undriven system while a 5D description is associated with the driven system. For an amplitude $A = 0.35$, the phase portraits obtained by integrating the 3D and 5D models are displayed in Figs. 10 and 11, respectively. The populations of periodic orbits are reported in Table 1. All evaluated linking numbers are found to be in agreement with those predicted by the linking matrix of Eq. (16). The 3D model is characterized by a kneading sequence encoded by (101) located at $x_\sigma = 0.6154$ which is very close to the one of the undriven Rössler system ($x_\sigma = 0.6109$). It means that the population of periodic orbits is slightly different from the one extracted from the

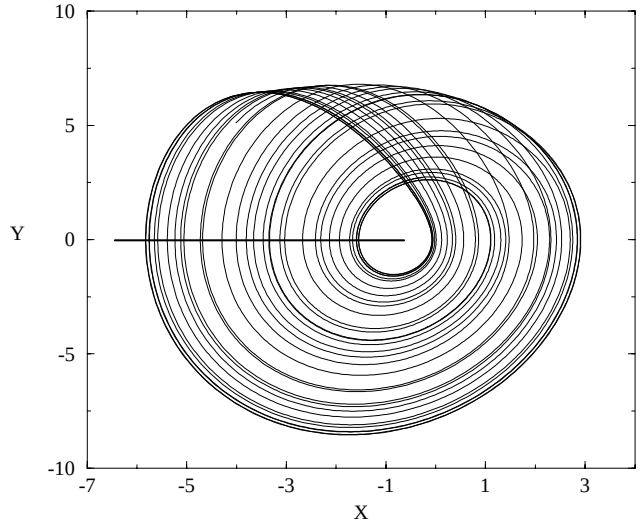

Fig. 10. Plane projection of the phase portrait obtained by integrating the three-variable model ($A = 0.35$). Modeling parameters are $(N_v, N_s, N_K) = (11, 9, 11)$.

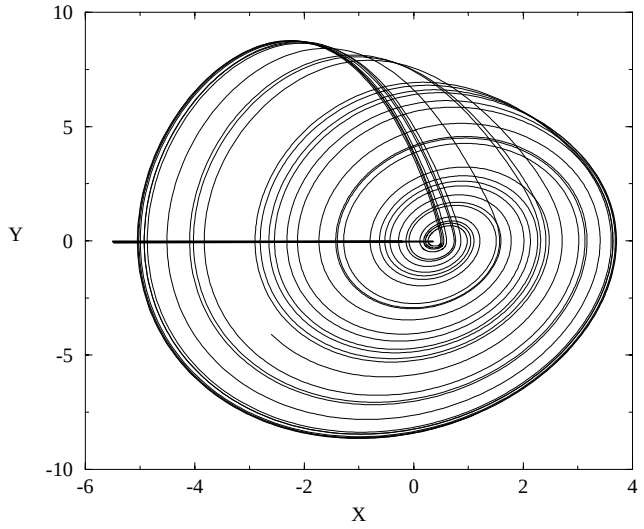

Fig. 11. Plane projection of the phase portrait obtained by integrating the five-variable model ($A = 0.35$). Modeling parameters are $(N_v, N_s, N_K) = (34, 20, 21)$.

undriven Rössler system (a few periodic orbits not extracted from the original Rössler system are embedded within the model attractor). By forcing the model to be 3D, the global vector field modeling technique provides a model which does not properly take into account the action of the external driving force on the dynamics. This actually works however pretty well because the driving force has a sufficiently small amplitude. In contrast, the 5D model is found to be perfectly equivalent to the driven Rössler system, having in particular the same population of periodic orbits (Table 1).

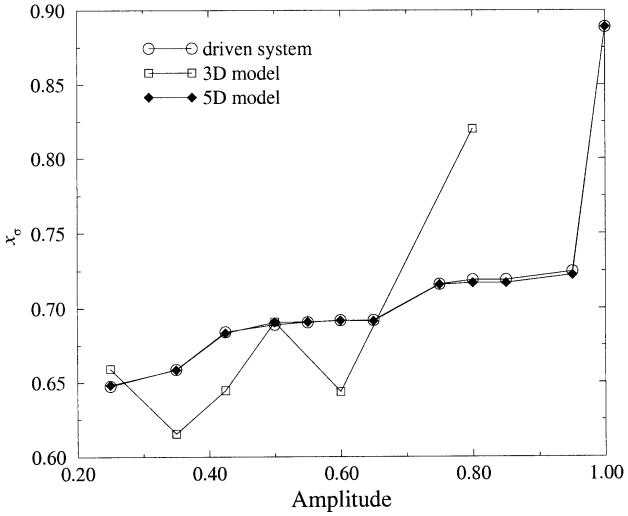

Fig. 12. Evolution of the kneading coordinate of the 3D and 5D models versus the amplitude A. Comparisons with the driven system.

For $A = 0.6$, the 3D-model obtained with modeling parameters $(N_v, N_p, N_K) = (31, 24, 30)$ is still close to the undriven Rössler system. Its population of periodic orbits is defined by a kneading orbit (100101) with symbolic coordinate $x_\sigma = 0.6438$ which is not very far from the symbolic coordinate $x_\sigma = 0.6109$ of the kneading sequence for the undriven Rössler system. Nevertheless, one may remark that the number of monomials involved in the estimated function $\tilde{F}(X, Y, Z, U, V)$ has significantly increased. Although the 3D models mainly capture the dynamics of the undriven system, i.e. filter the action of the driving force, 14 monomials are added in the estimated function $\tilde{F}(X, Y, Z, U, V)$ with respect to the 17 monomials involved in the exact function $F(X, Y, Z, U, V)$. These extra-monomials are required to obtain a successful model. One may then expect that, when the amplitude of the driving force increases too much, the filtering of the action of the driving force becomes inefficient. The validity of this statement may be appreciated by examining the evolution of the kneading sequences of the 3D and 5D models and of the driven system versus the amplitude as displayed in Fig. 12.

In particular, for $A = 0.5$, the populations of the 3D and 5D models obtained with modeling parameters (N_v, N_p, N_K) identical to (14, 14, 12) and (34, 11, 21) respectively, are both equal to the population of the driven system. Consequently, the population of periodic orbits of the 3D model is different from the one of the undriven system. 3D

models may then capture some effects of the driving force when the amplitude is sufficiently large, i.e. the modeling algorithm cannot be used to filter the action of the driving force when its amplitude is too large.

For $A = 0.6$, a 5D model, with modeling parameters set to (35, 10, 21), generates a chaotic behavior very similar to the one generated by the driven system, i.e. both behaviors are characterized by the same kneading sequence, as exhibited by the population of periodic orbits reported in Table 2. Two period-6 orbits are however lacking in the population of the 5D model. Such (minor) discrepancies are likely to arise from the limited amount of data used to extract periodic orbits. In fact, the agreement between kneading sequences of 5D models and of the driven system holds for all studied amplitudes (Fig. 12). Also, first-return maps for 5D models are always very similar to the one of the driven system. In particular, they always exhibit a thickness which compares very favorably to the one exhibited in Fig. 6. Nevertheless, for sufficiently large amplitude values, no 3D model can be obtained. Such a feature is in agreement with the previously evaluated embedding dimension since, for amplitude values greater than 0.5, the embedding dimension is at least equal to 4.

5. Conclusion

By investigating systems embedded in $\mathbb{R}^m$, driven by an external force $A\cos(\omega t+\varphi)$, we have demonstrated that the natural phase space (global phase space) of the driven systems has a dimension $m+2$ rather than $m+1$ for the usual extended phase space. The use of such a global phase space presents many advantages, one of them is that it enables to estimate successful global models. The present approach corresponds to a description of the processes generating the dynamics including those involved for generating the driving force. This description is particularly convenient when the driving force is not known or cannot be measured but it requires the input to be stationary in the sense that its main features can be described by a fixed model. Moreover, it has been exemplified, in the case when a sinusoidal force is applied to the third equation of the Rössler system, that the driven system is not always phase synchronized with the driving force. Deep consequences arise from such a feature. In particular, a Poincaré section cannot be conveniently identified to a stroboscopic representation of the dynamics as usually used in the analysis of driven systems. In such a case, the global phase space appears to be very convenient for analyzing such systems.

When the number of variables involved in the model corresponds to the number of variables spanning the global phase space, a global modeling technique provides models whose quality does not depend on the amplitude of the driving force. Conversely, when the number of variables involved in the model corresponds to the number of variables spanning the phase space associated with the undriven system, the obtained models rather reproduce the dynamics of the unforced system, although the driving force develops the observed dynamics of the driven system. In other words, when such a lower-dimensional model is attempted, the action of the driving force is not correctly captured by the model. The modeling technique acts like a sophisticated filter. Such a filtering effect is only observed up to a certain value of the amplitude ($A = 0.6$) beyond which no 3D model can be obtained.

Indeed, by using a global modeling technique in the global phase space starting from a y-time series of the driven Rössler system, we obtain successful 5D models for any amplitude value of the driving force. Although some difficulties (encoding periodic orbits) have been encountered when performing the topological characterization for large amplitudes, mainly due to the rough generating partition used, each model has been found to be topologically equivalent to the driven Rössler system. Moreover, we demonstrated that a topological analysis, only available in 3D spaces in utmost rigor, may be used for almost all amplitudes. Such a result may be understood by realizing that the additional two dimensions associated with the driving force correspond to an isolated 2D Hamiltonian subsystem, i.e. are only required to generate a limit cycle which is a trivial knot with a poor topological structure. Also, this topological characterization is actually achieved by projecting the 5D global phase space in a 3D subspace associated with the non-Hamiltonian process. In addition to that, one may be ensured that the results are not a consequence of the "reduced-dimension topological analysis" because it is performed for the original system and for the model in the same subspace of the 5D global phase space.

Acknowledgments

Oliver Ménard is supported by the *Région de Haute-Normandie*. We wish to thank the

anonymous referee who helped us to improve the quality of this paper.

References

Abarbanel, H. D. I. & Kennel, M. B. [1993] "Local false nearest neighbors and dynamical dimensions from observed chaotic data," *Phys. Rev.* **E47**(5), 3057–3068.

Aguirre, L. A. & Billings, S. A. [1994] "Validating identified nonlinear models with chaotic dynamics," *Int. J. Bifurcation and Chaos* **4**(1), 109–125.

Bergé, P., Pomeau, Y. & Vidal, Ch. [1984] *L'ordre dans le chaos* (Hermann, Paris).

Birman, J. S. & Williams, R. F. [1983] "Knotted periodic orbits in dynamical systems II: Knot holders for fibered knots," *Contemp. Math.* **20**, 1–60.

Boulant, G., Lefranc, M., Bielawski, S. & Derozier, D. [1997] "Horseshoe templates with global torsion in a driven laser," *Phys. Rev.* **E55**(5), 5082–5091.

Brown, R., Rul'kov, N. F. & Tracy, E. R. [1994] "Modeling and synchronizing chaotic systems from time-series data," *Phys. Rev.* **E49**(5), 3784–3800.

Cao, L. [1997] "Practical method for determing the minimum embedding dimension of a scalar time series," *Physica* **D110**(1 & 2), 43–52.

Collet, P. & Eckmann, J. P. [1980] "Iterated maps on the interval as dynamical systems," in *Progress in Physics*, eds. Jaffe, A. & Ruelle, D. (Birkhäuser, Boston).

Crutchfield, J. P. & McNamara, B. S. [1987] "Equations of motion from a data series," *Complex Syst.* **1**, 417–452.

Dutertre, P. [1995] "Caractérisation des attracteurs étranges par la population d'orbites périodiques," PhD dissertation, Université de Rouen, France.

Fang, H. P. [1994] "Dynamics of strongly dissipative systems," *Phys. Rev.* **E49**(6), 5025–5031.

Fang, H. P. [1995] "Universal bifurcation property of two- or higher-dimensional dissipative systems in parameter space: Why does 1D symbolic dynamics work so well?" *J. Phys.* **A28**, 3901–3910.

Farmer, J. D. & Sidorowitch, J. J. [1987] "Predicting chaotic time series," *Phys. Rev. Lett.* **59**(8), 845–848.

Flepp, L., Holzner, R., Brun, E., Finardi, M. & Badii, R. [1991] "Model identification by periodic-orbit analysis for NMR-laser chaos," *Phys. Rev. Lett.* **67**(17), 2244–2247.

Gilmore, R. & McCallum, J. W. L. [1995] "Structure in the bifurcation diagram of the Duffing oscillator," *Phys. Rev.* **E51**(2), 935–956.

Gouesbet, G. & Letellier, C. [1994] "Global vector field reconstruction by using a multivariate polynomial L_2-approximation on nets," *Phys. Rev.* **E49**(6), 4955–4972.

Gouesbet, G. & Maquet, J. [1992] "Construction of phenomenological models from numerical scalar time series," *Physica* **D58**, 202–215.

Grassberger, P., Kantz, H. & Mœning, U. [1989] "On the symbolic dynamics of the Hénon map," *J. Phys. A: Math. Gen.* **22**, 5217–5230.

Hall, T. [1994] "The creation of Horseshoes," *Nonlinearity* **7**(3), 861–924.

Le Sceller, L., Letellier, C. & Gouesbet, G. [1994] "Algebraic evaluation of linking numbers of unstable periodic orbits in chaotic attractors," *Phys. Rev.* **E49**(5), 4693–4695.

Letellier, C. [1994] "Caractérisation topologique et reconstruction d'attracteurs étranges," PhD dissertation, Université de Paris VII.

Letellier, C. & Gouesbet, G. [1996] "Topological characterization of reconstructed attractors modding out symmetries," *J. Phys. II* **6**, 1615–1638.

Letellier, C., Le Sceller, L., Dutertre, P., Gouesbet, G., Fei, Z. & Hudson, J. L. [1995] "Topological characterization and global vector field reconstruction from an experimental electrochemical system," *J. Phys. Chem.* **99**, 7016–7027.

Letellier, C., Ringuet, E., Maheu, B., Maquet, J. & Gouesbet, G. [1997] "Global vector field reconstruction of chaotic attractors from one unstable periodic orbit," *Entropie* **202/203**, 147–153.

Mausbach, T., Klinger, T. & Piel, A. [1999] "Chaos and chaos control on a strongly driven thermoionic plasma diode," *Physics of Plasma*, in press.

Mindlin, G. B. & Gilmore, R. [1992] "Topological analysis and synthesis of chaotic time series," *Physica* **D58**, 229–242.

Mindlin, G. B., Solari, H. G., Natiello, M. A., Gilmore, R. & Hou, X. J. [1991] "Topological analysis of chaotic time series data from the Belousov–Zhabotinski reaction," *J. Nonlin. Sci.* **1**, 147–173.

Rice, J. R. [1964] *The Approximation of Functions*, Vol. 1 (Addison-Wesley, MA); [1969] Vol. 2.

Tufillaro, N. B., Abbott, T. & Reilly, J. [1992] *An Experimental Approach to Non Linear Dynamics and Chaos* (Addison-Wesley, NY).

Tufillaro, N. B., Wyckoff, P., Brown, R., Schreiber, T. & Molteno, T. [1995] "Topological time series analysis of a string experiment and its synchronized model," *Phys. Rev.* **E51**(1), 164–174.

Wiggins, S. [1980] "Introduction to applied nonlinear dynamical systems and chaos," *Texts in Applied Mathematics* **2** (Springer-Verlag).